Global Analysis of Unmatched Polarized Fluorescence Decay Curves of Systems Exhibiting a Residual Anisotropy at Long Times

ARTICLE *in* THE JOURNAL OF PHYSICAL CHEMISTRY · JUNE 1996

Impact Factor: 2.78 · DOI: 10.1021/jp960085j

5 AUTHORS, INCLUDING:

GB Dutt
Bhabha Atomic Research Centre
75 PUBLICATIONS **1,636** CITATIONS
SEE PROFILE

Marcel Ameloot
Hasselt University
220 PUBLICATIONS **3,494** CITATIONS
SEE PROFILE

Delia Bernik
University of Buenos Aires
43 PUBLICATIONS **510** CITATIONS
SEE PROFILE

Frans C De Schryver
University of Leuven
671 PUBLICATIONS **21,236** CITATIONS
SEE PROFILE

Global Analysis of Unmatched Polarized Fluorescence Decay Curves of Systems Exhibiting a Residual Anisotropy at Long Times

G. Bhaskar Dutt,[†] Marcel Ameloot,*[,‡] Delia Bernik,[†,§] R. Martín Negri,[†,§] and Frans C. De Schryver*[,†]

Laboratorium voor Moleculaire Dynamica en Spectroscopie, Departement Scheikunde, Katholieke Universiteit Leuven, Celestijnenlaan 200-F, B-3001 Leuven (Heverlee), Belgium, and Limburgs Universitair Centrum, Universitaire Campus, B-3590 Diepenbeek, Belgium

Received: January 4, 1996[⊗]

A previous study of the performance of the global, i.e., simultaneous, analysis of unmatched polarized decay traces [Crutzen, M.; et al. *J. Phys. Chem.* **1993**, *97*, 8133] is extended for the time-dependent anisotropy $r(t)$, given by $r(t) = \beta \exp(-t/\Phi) + r_\infty$. The evaluation was done with computer-generated and experimentally collected data. Two different schemes of analysis of unmatched polarized decay traces were considered. In scheme A the decay curves measured with the analyzer set at 0°, 54.7°, and 90° with respect to the polarization of the incident light were globally analyzed, while only the traces at 0° and 90° were taken into account in scheme B. Data were simulated for various Φ/τ ratios (0.1, 1, 3, and 10). The value obtained for the fluorescence lifetime τ was accurate and precise for all cases considered. For $\Phi/\tau = 0.1$, 1, and 3 ($\tau = 5$ ns) the parameters β and Φ were well recovered. The accuracy and precision were very similar to the results obtained with matched decay traces. The recovery of r_∞ was case dependent. Scheme A performed somewhat better than scheme B. When r_0 was fixed to the true value, the analysis with schemes A and B yielded the same accuracy and precision as the analysis of the matched curves. For $\Phi/\tau = 10$, the parameter estimates for the anisotropy parameters were inaccurate and suffered from very high uncertainty. No improvement was obtained when r_0 and the matching factors were kept fixed to the true value. This is in contrast with the results obtained for $r(t)$ without an r_∞ term, where Φ/τ can even be much higher when r_0 or the matching factors are kept fixed. There was some improvement when the signal to noise ratio was increased. When the decay of the total fluorescence was biexponential, scheme A performed much better than scheme B. The best results were obtained when G or r_0 was kept fixed. It was found that with respect to the normalization of the polarized decay traces the fundamental anisotropy r_0 and the matching factor G contain the same information. In general, the best accuracy and precision in the parameter recovery were obtained when a predetermined value for G or r_0 was used in the analysis. The performance of the analyses without the information on r_0 or G depended more on the Φ/τ ratio than for the analyses where this information was used. Fixing of both G and r_0 to the proper value might lead to an improved precision. It has to be emphasized that the use of incorrect values for G (with r_0 freely adjustable) or r_0 (with G freely adjustable) could lead to good data fits, although the parameter estimates are incorrect. A small change in r_0 can lead to a large change in Φ. Therefore, in general it can be recommended that either G or r_0 be fixed, but not both. Alternatively, the comparison of the results obtained with a freely adjustable G and a fixed G can provide a check for the data analysis.

Introduction

The method of time-resolved fluorescence depolarization allows the study of the rotational dynamics of fluorescent molecules in isotropic solvents,[1−5] micelles,[6,7] polymers,[8] and lipid vesicles.[1,2,9−14] The information on the rotational motion is contained in the fluorescence anisotropy decay $r(t)$ after δ pulse excitation,

$$r(t) = \frac{i_{||}(t) - i_{\perp}(t)}{i_{||}(t) + 2i_{\perp}(t)} \tag{1}$$

where $i_{||}(t)$ and $i_{\perp}(t)$ denote the polarized fluorescence decays with the emission polarizer set parallel and perpendicular, respectively, to the polarization direction of the excitation light, which is perpendicular to the excitation−detection plane. The polarized intensities can be written as

$$i_{||}(t) = (^1/_3)f(t)[1 + 2r(t)] \tag{2}$$

$$i_{\perp}(t) = (^1/_3)f(t)[1 - r(t)] \tag{3}$$

with $f(t)$ being the decay of the total fluorescence.

It will be assumed in this paper that $f(t)$ can be written as

$$f(t) = \sum_{i=1}^{n} \alpha_i \exp(-t/\tau_i) \tag{4}$$

For an excited species in a single type of isotropic environment, $r(t)$ is, in general, given by a linear combination of exponentially decaying functions:

* Author to whom correspondence should be addressed.
† Katholieke Universiteit Leuven.
‡ Limburgs Universitair Centrum.
§ Current address: Lab. de Fotoquimica, Depto Quimica Exactas, Cindad Universitaria, Pabellon II−1er. P, 1428 Buenos Aires, Argentina.
⊗ Abstract published in *Advance ACS Abstracts,* May 15, 1996.

S0022-3654(96)00085-8 CCC: $12.00

$$r(t) = \sum_{j=1}^{m} \beta_j \exp(-t/\Phi_j) \quad (5)$$

The value of the anisotropy at $t = 0$ is given by the sum of the preexponentials β_j and will be denoted by r_0.

When the motion of the rotating molecule is restricted by a hindering potential, $r(t)$ does not relax to zero value.[1,2,9,15−21] This means that in eq 5 at least one rotational correlation time Φ_j takes a very large value compared to the relaxation times τ_i. The residual anisotropy at long times will be denoted as r_∞.

In the case of a mixture of species and/or environments, $i_{||}(t)$ and $i_\perp(t)$ can generally be written as[22−24]

$$i_{||}(t) = (^1/_3)\sum_{i=1}^{n} \alpha_i \exp(-t/\tau_i)[1 + 2\sum_{j=1}^{m} L_{ij}\beta_j \exp(-t/\Phi_j)] \quad (6a)$$

$$i_\perp(t) = (^1/_3)\sum_{i=1}^{n} \alpha_i \exp(-t/\tau_i)[1 - \sum_{j=1}^{m} L_{ij}\beta_j \exp(-t/\Phi_j)] \quad (6b)$$

where the factors L_{ij} are equal to unity if the relaxation time τ_i is associated with the correlation time Φ_j and zero otherwise.

For an arbitrary orientation θ of the emission polarizer, the corresponding polarized intensity $i(\theta,t)$ can be written as[24]

$$i(\theta,t) = (^1/_3)\sum_{i=1}^{n} \alpha_i \exp(-t/\tau_i)[1 + (3\cos^2\theta - 1)\sum_{j=1}^{m} L_{ij}\beta_j \times \exp(-t/\Phi_j)] \quad (7)$$

At $\theta = 54.7°$, the so-called magic angle, $i(54.7°,t) = f(t)/3$.

Polarized intensity decays can be collected by the single-photon timing technique in the time domain and by phase and modulation fluorometry in the frequency domain.[1,25−27] This paper focuses on the single-photon timing technique. In this method the collected polarized fluorescence decays, $I_{||}(t)$ and $I_\perp(t)$, are convolution products of $i_{||}(t)$ and $i_\perp(t)$ with the instrumental response function.

Several methods have been described to recover the parameters α_i, τ_i, β_j, and Φ_j from the measured polarized intensities.[23,24,28−38] One of the best methods is the global analysis approach, in which the polarized intensity decays are analyzed simultaneously by linking parameters that are common to the different fitting functions.[23,24,31,35,36] The global analysis approach has several advantages. The usual weighting factors for single-photon timing experiments based upon the Poisson (counting) statistics can be used directly. All parameters of both $f(t)$ and $r(t)$ are optimized simultaneously in a single-step analysis. The excitation profiles and the instrument response for the polarized intensity decay curves may be different, allowing for several simultaneous detection channels. Furthermore, several experimental conditions can be changed in the collection of polarized intensity decays, such as excitation/emission wavelength, orientation of the emission polarizer, and different timing calibrations. The corresponding global analysis allows for enhanced parameter recovery and model discrimination.

In a global analysis of polarized intensity decays, the following linking schemes can be utilized. The preexponential factors β_j can be linked along any experimental axis except the excitation wavelength axis, where different transitions are involved. However, the rotational correlation times can be linked along the excitation/emission wavelength axis. This approach has proved its usefulness in resolving closely spaced rotational correlation times.[23,35] The preexponential factors α_i of the total fluorescence decay of a heterogeneous system in general depend on the excitation and emission wavelengths. All parameters τ_i, β_j, and Φ_j and the ratios of α_i can be linked when different timing calibrations are used to improve the recovery of widely different relaxation times.

In an experimental environment, the collected polarized intensity decays are not likely to be properly matched due to the polarization bias of the apparatus, fluctuations in excitation pulse intensity, and differences in collection time. The experimental and deconvoluted polarized intensity, $i^e(\theta,t)$, is related to the ideal and matched intensity, $i(\theta,t)$, by

$$i^e(\theta,t) = \kappa(\theta)\, i(\theta,t) \quad (8)$$

where $\kappa(\theta)$ are the matching factors, which are generally time independent. Therefore, the α_i values of the decay traces taken at different analyzer angles can be linked. In the analysis, $\kappa(\theta)$ can be a freely adjustable parameter. Several implementations are possible: (a) all $\kappa(\theta)$ but one and all α_i are freely adjustable, while the remaining $\kappa(\theta)$ is fixed at an arbitrary value; (b) all α_i but one and all $\kappa(\theta)$ are freely adjustable, while the remaining α_i is fixed at some arbitrary value. To reduce the number of fitting parameters, matching factors can be determined experimentally.[30] However, as polarized intensity decays can be collected under various conditions, a full set of matching factors has to be measured to allow for a global analysis of the decay data surface.

In a previous report,[24] we evaluated the global analysis of unmatched polarized fluorescence decay curves.[32,34,36] It was shown that good parameter recovery was obtained when the various matching factors were freely adjustable parameters. However, the cases considered did not include an r_∞ term. It can be expected that the presence of an r_∞ term might complicate the analysis with freely adjusting matching factors. Indeed, in the limiting case where there is no rotational motion at all, the information about the anisotropy is contained in a single variable, whose contribution in $i(\theta,t)$ will lead to a parameter that will lump together with $\kappa(\theta)$. Therefore, the matching factors have to be known to obtain information about the anisotropy. In the case where there is rotational motion without hindering potential, the anisotropy contributes to the time dependence of $i(\theta,t)$. The datum at each point in time can be seen as giving rise to an additional equation that has to be satisfied by the fitting parameters. The linking of the anisotropy parameters over these equations provides sufficient constraints, allowing the matching factors to be freely adjustable. The case of a time-dependent anisotropy with an r_∞ term is somewhat intermediate between the two cases described earlier.

The purpose of this paper is to investigate the performance of the global analysis of unmatched fluorescence decay curves that contain an r_∞ term. The evaluation is done with computer-generated and experimentally collected data.

Theory

Matching Factors. Experimentally, the method of determining the matching factors depends on the experimental setup and the different axes in the decay data surface. In many cases, it suffices to determine $i_{||}(t)$ and $i_\perp(t)$ to obtain good estimates for the parameters in the expression of $r(t)$. The experimental and deconvoluted polarized intensities, $i_{||}^e(t)$ and $i_\perp^e(t)$, are related to the theoretical curves as follows:

$$i_{||}^e(t) = \kappa(0°)\, i_{||}(t) \quad (9a)$$

$$i_\perp^e(t) = \kappa(90°)\, i_\perp(t) \quad (9b)$$

The anisotropy $r(t)$ can be written as

$$r(t) = \frac{G i_{\parallel}^{e}(t) - i_{\perp}^{e}(t)}{G i_{\parallel}^{e}(t) + 2 i_{\perp}^{e}(t)} \quad (10)$$

where

$$G = \kappa(90°)/\kappa(0°) \quad (11)$$

If the decays are collected for the same number of absorbed photons, the matching factor G has to correct only for the polarization bias in the detection system. For macroscopically isotropic samples, the polarization bias can be determined as follows. For the assumed symmetry of the sample, the polarized intensities measured with the excitation polarizer oriented horizontally should all be equal in principle, irrespective of the orientation of the emission polarizer. The matching of $i_{\parallel}^{e}(t)$ and $i_{\perp}^{e}(t)$ is then accomplished by determining $G = G_H$:

$$G_H = I_{HH}/I_{HV} \quad (12)$$

where I_{HV} and I_{HH} denote the polarized steady-state intensities observed with the excitation polarizer set horizontally and the emission polarizer oriented horizontally and vertically, respectively.

In the more general case, the matching factor can be determined from the steady-state anisotropy $\langle r \rangle$ measured under identical conditions and appropriately corrected for any mismatch between the steady-state polarized intensities:

$$\langle r \rangle = \int_0^\infty r(t)\, f(t)\, dt \Big/ \int_0^\infty f(t)\, dt \quad (13)$$

The matching factor $G = G_f$ based on $\langle r \rangle$ is given by[30]

$$G_f = \frac{1 + 2\langle r \rangle}{1 - \langle r \rangle}\left[\int_0^\infty i_{\perp}^{e}(t)\, dt \Big/ \int_0^\infty i_{\parallel}^{e}(t)\, dt\right] \quad (14)$$

It can be shown (e.g., by using Laplace transforms) that the ratio of the integrals appearing in eq 14 can also be determined from the total number of counts of the nondeconvoluted and noncorrected experimental decays $I_{\parallel}^{e}(t)$ and $I_{\perp}^{e}(t)$, provided that the time window of observation is wide enough and that the instrument response functions for both polarizations exhibit the same time dependence.

In the global analysis with freely adjustable factors $\kappa(0°)$ and $\kappa(90°)$, it is actually possible to determine G from the parameter estimates if the preexponential factors α_i are linked. The corresponding value will be denoted by G_r. Obviously, in the analysis when $\kappa(0°)$ is fixed to unity, G_r is given by the estimate for $\kappa(90°)$.

For simulations, the factor G is known and will be denoted by G^t. In these cases G_f and G_r can be readily compared with G^t to check the performance of the global analysis with freely adjustable factors $\kappa(0°)$ and $\kappa(90°)$.

Materials and Methods

Materials and Sample Preparation. *all-trans*-1,6-Diphenyl-1,3,5-hexatriene (DPH), dipalmitoylphosphatidylcholine (DPPC), and the buffer Tris-HCl were obtained from Sigma Chemical Co. and used as received. Chloroform and ethanol were bought from Merck. 1,4-Bis(5-phenyloxazol-2-yl)benzene (POPOP) (laser grade) was obtained from Kodak.

DPH-loaded small unilamellar vesicles (SUV) were prepared by codissolving lipid and probe in chloroform and evaporating the solvent onto the sides of the flasks by using a nitrogen stream. The dry film was dispersed in 10 mM Tris-HCl (pH 7.4) at temperatures above the phase transition of the lipids. The dispersion was sonicated under a N_2 stream at 50 °C with a tip-sonicator (W-375 Heat Systems-Ultrasonic, Inc.) until a clear suspension was obtained. Ti debris of the sonicator tip was removed by subsequent centrifugation. The final concentration of lipid was 7×10^{-4} M, with a lipid/fluorophore ratio of 400/1. The experiments were conducted by using 1 cm cells.

Instrumentation. Steady-state fluorescence measurements were carried out with an SLM-8000C spectrofluorometer. The fluorometer was equipped with excitation and emission polarizers. The anisotropy determinations were performed in the L-format configuration. The temperature was controlled with a Lauda RUL 480 thermostat−cryostat.

Polarized intensity decays were collected by the single-photon timing technique using a Spectra Physics cavity-dumped mode-locked synchronously pumped R6G dye laser system. The system is described in detail elsewhere.[24,40] The specific features are repeated here. The polarized intensity decays of the sample can be measured at any angle of the emission polarizer, which is controlled by the computer. A circular variable neutral-density filter (RosOptics Z06,011, mat FS, OD 0−3) in the emission path is adjusted by the computer so that all decay traces are collected at the same detection rate. The decay data of the sample and the reference are collected alternately for preset dwell times. The decay traces of the reference compound are measured with the emission polarizer set at 54.7°.

All calculations and synthetic data generations were performed on an IBM 6150-125 computer in single precision.

Data Analysis. The analysis program and procedures have been described elsewhere.[24] The main features are repeated here for the convenience of the reader. The polarized intensity curves $i(\theta,t)$ were analyzed according to

$$i(\theta,t) = \kappa(\theta)/3 \sum_{i=1}^{n} \alpha_i \exp(-t/\tau_i)\left[1 + (3\cos^2\theta - 1)\sum_{j=1}^{m} L_{ij}\beta_j \times \exp(-t/\Phi_j)\right] \quad (15)$$

The program has the possibility to constrain the sum of the β_j values to a given value for r_0. r_0 can be different for each τ_i. In the analyses, all corresponding parameters of $f(t)$ and $r(t)$, including the preexponentials α_i, were linked over traces corresponding to various values of the angle θ. The matching factor $\kappa(0°)$ was kept fixed at unity while the remaining $\kappa(\theta)$ were freely adjustable.

The reference convolution method[41−45] was used. The lifetime of the reference decay, τ_r, was a freely adjustable parameter.

The anisotropy analysis program is part of a global analysis program that was described earlier in detail.[46] A global, reweighted iterative reconvolution program based on the nonlinear least-squares algorithm of Marquardt[47] was used to estimate the unknown parameters. The fitting parameters were determined by minimizing the global reduced chi-square χ_g^2

$$\chi_g^2 = \sum_{k}^{q} \sum_{i} w_{ki}(I^{o}_{ki} - I^{c}_{ki})^2/\nu \quad (16)$$

where the index k sums over q experiments, the index i sums over the appropriate channel limits for each individual experiment, and w_{ki} are the weighting factors.[48] I^{o}_{ki} and I^{c}_{ki} denote the observed (experimentally measured or computer-generated) and calculated values, respectively, corresponding to the ith channel of the kth experiment. ν represents the number of degrees of freedom for the entire multidimensional fluorescence decay surface.

TABLE 1: Schemes for the Global Analysis of the Polarized Intensity Decay Curves $I^e(\theta, t)$

scheme	considered angles θ (deg)	$\kappa(0°)$[c]	$\kappa(90°)$	$\kappa(54.7°)$
A[a]	0, 90, 54.7	1	free	free
B	0, 90	1	free	−
C_1[b]	0, 90	1	G_f (fixed)	−
C_2	0, 90	1	G^t (fixed)	−

[a] In some cases the third angle (54.7°) in scheme A is replaced by another value. [b] In some cases $\kappa(90°)$ is fixed to a value different from G_f. [c] $\kappa(0°)$ is kept fixed to unity.

Schemes for Global Analysis of Polarized Fluorescence Decays. Sets of polarized intensity decay curves were analyzed simultaneously according to various schemes (Table 1). In all schemes $\kappa(0°)$ was kept fixed to unity. The preexponential factors α_i were linked over all decay curves and freely adjustable in all schemes. In scheme A the curves $I^e(0°,t)$, $I^e(90°,t)$, and $I^e(54.7°,t)$ are analyzed simultaneously with $\kappa(90°)$ and $\kappa(54.7°)$ freely adjustable. Scheme B is essentially equal to scheme A, the only difference being that the curve $I(54.7°,t)$ is not included in the simultaneous analysis. In schemes C_1 and C_2, the properly matched curves $I^e(0°,t)$ and $I^e(90°,t)$ are globally analyzed, i.e., $\kappa(0°)$ is fixed to unity and $\kappa(90°)$ is kept fixed to G_f and G^t in schemes C_1 and C_2, respectively.

Synthetic Data Generation. The synthetic decay traces were generated by convolution of the expressions for $i(\theta,t)$ with a nonsmoothed measured instrument response function. Reference decays were synthesized by convolution of a single exponential ($\tau_r = 1$ ns) with the instrument response function used for the sample decays. Poisson noise was added to the simulated curves. For each curve a different seed for the random number generator was used. Unless noted otherwise, all simulated decays had 500 data channels and about 10^4 counts in the peak channel. More details of the decay data simulations are given elsewhere.[48] In the tables the simulation parameters are indicated by the superscript t.

Results and Discussion

Simulations. The value of the reference lifetime was always well recovered for every linking scheme. Therefore, the value of the reference lifetime is not tabulated. Fixing of the reference lifetime did not improve the recovery of the remaining parameters. Note that in the various analyses $\kappa(0°)$ was always kept fixed to unity so that $G_r = \kappa(90°)$.

CASE 1: $f(t) = \alpha\ exp(-t/\tau)$ and $r(t) = r_0\ exp(-t/\Phi)$. In a previous report,[24] we discussed parameter recovery in the case of a vanishing anisotropy at long times. However, the values recovered for the factors $\kappa(\theta)$ were not explicitly illustrated. To demonstrate the performance of the global analysis in this aspect and to allow comparison with the cases with nonvanishing anisotropy, the following case was simulated: $n = 1$, $m = 1$, $\tau^t = 5$ ns, $\Phi^t = 5$ ns, and $r_0{}^t = 0.3$. The time increment per channel was 62 ps. The reference lifetime $\tau_r{}^t$ was 1 ns. Three different values for G^t were considered: 1, 0.5, and 2 (Table 2). By using schemes A, B, and C_1, G_r and the parameters of $f(t)$ and $r(t)$ were well recovered and comparable with those obtained with scheme C_2. This was independent of the value of G^t.

CASE 2: $f(t) = \alpha\ exp(-t/\tau)$ and $r(t) = (r_0 - r_\infty)\ exp(-t/\Phi) + r_\infty$ with $\Phi^t/\tau^t = 1$. Polarized intensity decay curves with nonvanishing anisotropy at long times were simulated by using the values $\tau^t = 5$ ns, $\Phi^t = 5$ ns, $r_0{}^t = 0.30$, $r_\infty{}^t = 0.20$ ($\beta^t = r_0{}^t - r_\infty{}^t = 0.1$), $\tau_r{}^t = 1$ ns, and $G^t = 1.0$. Various time increments were used: 50, 55, 62, 80, and 100 ps. One can define δ as (number of counts in the last channel/number of counts at the peak channel of the nondeconvolved decay) × 100. The results obtained with linking scheme B by using the constraint $r_0 = 0.3$ as a function of δ are shown in Table 3. The results associated with the same time increment per channel correspond to decay traces generated by using different seed numbers. The parameter estimates are in good agreement with the simulation values for all time increments considered. For the time

TABLE 2: Recovered Parameters of a Monoexponential $f(t)$ and a Monoexponential $r(t)$[a]

scheme	τ (ns)	Φ (ns)	r_0	$G_r = \kappa(90°)$	χ_g^2
		Case A: $G^t = 1$			
A	4.989	5.1	0.300	1.002	1.013
	(0.004)	(0.1)	(0.002)	(0.007)	
B	4.989	5.1	0.300	1.000	1.026
	(0.005)	(0.1)	(0.002)	(0.007)	
C_1	4.988	4.94	0.298	0.992[b]	1.027
	(0.005)	(0.05)	(0.002)		
C_2	4.989	5.05	0.300	1[c]	1.025
	(0.005)	(0.05)	(0.002)		
		Case B: $G^t = 0.5$			
A	4.985	4.9	0.294	0.492	0.987
	(0.005)	(0.1)	(0.003)	(0.004)	
B	4.984	4.9	0.294	0.493	0.971
	(0.006)	(0.1)	(0.003)	(0.004)	
C_1	4.986	4.98	0.296	0.496[b]	0.971
	(0.006)	(0.06)	(0.002)		
C_2	4.988	5.10	0.298	0.5[c]	0.974
	(0.006)	(0.06)	(0.002)		
		Case C: $G^t = 2.0$			
A	4.987	5.05	0.301	2.00	0.969
	(0.004)	(0.09)	(0.002)	(0.01)	
B	4.989	5.05	0.301	2.00	1.022
	(0.004)	(0.09)	(0.002)	(0.01)	
C_1	4.990	5.00	0.300	1.995[b]	1.021
	(0.004)	(0.04)	(0.001)		
C_2	4.989	5.04	0.301	2[c]	1.021
	(0.004)	(0.04)	(0.001)		

[a] $\tau^t = 5$ ns, $\Phi^t = 5$ ns, $r_0{}^t = 0.3$, $\tau_r{}^t = 1$ ns. Time increment per channel = 62 ps. Standard deviations of the parameter estimates are given in parentheses. [b] $\kappa(90°)$ was kept fixed to G_f (eq 14). [c] $\kappa(90°)$ was kept fixed to G^t.

TABLE 3: Influence of δ[a] on the Recovered Parameters of a Monoexponential $f(t)$ and a Monoexponential $r(t)$ with a Nonvanishing r_∞[a]

ti[d] (ps)	δ[b]	τ (ns)	β	Φ (ns)	r_∞	$G_r = \kappa(90°)$	χ_g^2
50	1.2	4.998	0.102	5.3	0.198	1.005	0.982
		(0.005)	(0.002)	(0.3)	(0.002)	(0.004)	
	1.2	5.001	0.103	5.0	0.197	0.992	1.053
		(0.005)	(0.002)	(0.3)	(0.002)	(0.004)	
55	0.7	4.997	0.099	5.2	0.201	1.002	1.082
		(0.005)	(0.002)	(0.3)	(0.002)	(0.004)	
	0.9	4.997	0.100	4.9	0.200	1.002	0.897
		(0.005)	(0.002)	(0.3)	(0.002)	(0.004)	
62	0.5	4.988	0.101	4.9	0.199	0.999	1.122
		(0.005)	(0.002)	(0.3)	(0.002)	(0.005)	
	0.4	4.999	0.097	5.1	0.203	1.011	1.002
		(0.005)	(0.002)	(0.3)	(0.002)	(0.004)	
80	0.1	4.983	0.099	5.0	0.201	1.001	1.098
		(0.005)	(0.002)	(0.4)	(0.002)	(0.005)	
	0.1	4.987	0.101	5.3	0.199	1.008	0.966
		(0.005)	(0.002)	(0.4)	(0.002)	(0.005)	
100	0	4.993	0.104	5.0	0.196	0.989	1.070
		(0.006)	(0.003)	(0.4)	(0.003)	(0.005)	
	0	4.981	0.098	5.4	0.202	1.011	1.045
		(0.006)	(0.003)	(0.4)	(0.003)	(0.005)	

[a] Analysis scheme B was used and r_0 was fixed to the true value (see footnote *c*). [b] δ = (number of counts in the last channel)/(number of counts at the peak channel of the nondeconvoluted decay) × 100. [c] $\tau^t = 5$ ns, $\Phi^t = 5$ ns, $r_0{}^t = 0.3$, $r_\infty{}^t = 0.20$, $\tau_r{}^t = 1$ ns, and $G^t = 1$. Standard deviations of the parameter estimates are given in parentheses. [d] ti: time increment per channel.

TABLE 4: Recovered Parameters of a Monoexponential $f(t)$ and a Monoexponential $r(t)$ with a Nonvanishing r_∞ and $\Phi^t/\tau^t = 1$[a]

scheme	τ (ns)	β	Φ(ns)	r_∞	$G_r = \kappa(90°)$	χ_g^2
			Case A: r_0 Is Freely Adjustable			
A	4.996	0.101	4.9	0.18	0.94	1.068
	(0.005)	(0.002)	(0.3)	(0.02)	(0.06)	
B	4.99	0.101	4.8	0.19	1.0	1.123
	(0.01)	(0.002)	(0.3)	(0.07)	(0.2)	
C_1	4.998	0.101	4.9	0.200	1.002	1.122
	(0.005)	(0.002)	(0.3)	(0.002)		
C_2	4.998	0.101	4.9	0.200	1	1.122
	(0.005)	(0.002)	(0.3)	(0.002)		
			Case B: r_0 Is Fixed to the True Value			
A	4.994	0.102	4.9	0.198	0.998	1.068
	(0.004)	(0.002)	(0.3)	(0.002)	(0.004)	
B	4.998	0.101	4.9	0.199	0.999	1.122
	(0.005)	(0.002)	(0.3)	(0.002)	(0.005)	
C_1	4.988	0.101	5.1	0.199	1.002	1.122
	(0.005)	(0.002)	(0.2)	(0.002)		
C_2	4.988	0.101	5.0	0.199	1	1.121
	(0.005)	(0.002)	(0.2)	(0.002)		

[a] $\tau^t = 5$ ns, $\Phi^t = 5$ ns, $r_0{}^t = 0.3$, $\beta^t = 0.1$, $r_\infty{}^t = 0.20$, $\tau_r{}^t = 1$ ns, and $G^t = 1$. Time increment is 62 ps. Standard deviations of the parameter estimates are given in parentheses.

increments of 50 and 100 ps, 10 pairs of $I^e(0°,t)$ and $I^e(90°,t)$ were simulated by using the same set of simulation values, but with different seeds for the random number generator. For the time increment of 50 ps, the average values and corresponding standard deviations were $\tau = 4.996$ (0.003) ns, $\Phi = 5.0$ (0.2) ns, $\beta = 0.099$ (0.002), $r_\infty = 0.201$ (0.002), $\tau_r = 0.999$ (0.002) ns, and $G_r = 1.001$ (0.004). For the time increment of 100 ps, the average values and corresponding standard deviations were $\tau = 4.982$ (0.005) ns, $\Phi = 4.9$ (0.2) ns, $\beta = 0.099$ (0.002), $r_\infty = 0.201$ (0.002), $\tau_r = 0.991$ (0.003) ns, and $G_r = 0.999$ (0.006). These two sets of average values compare well with the values displayed in Table 3, implying that the standard deviations obtained at the end of the least-squares search are reliable.

At shorter time increments or larger values of τ^t and Φ^t, the ratio of the counts in the last channel to the number of counts at the peak, δ, increases. Simulations were also performed by using the values $\tau^t = 8$ ns, $\Phi^t = 8$ ns, $r_0{}^t = 0.3$, $r_\infty{}^t = 0.20$ ($\beta^t = 0.10$), $\tau_r{}^t = 1$ ns, and $G^t = 1.0$. The values of the time increments were 50, 55, 62, 80, and 100 ps so that the corresponding values for δ were 0.06, 0.05, 0.03, 0.01, and 0.004, respectively. Also for these sets of decay traces a good recovery of the parameters was obtained (results not shown).

To investigate the effect of constraining the sum of β and r_∞ to a given value for r_0, the decay curves simulated with $\tau^t = 5$ ns, $\Phi^t = 5$ ns, $r_0{}^t = 0.3$, $r_\infty{}^t = 0.20$ ($\beta^t = 0.10$), $\tau_r{}^t = 1$ ns, and $G^t = 1.0$ at a time increment of 62 ps (see Table 3) were reanalyzed with both β and r_∞ freely adjustable, and this using the various schemes is shown in Table 1. The results for the unconstrained and constrained analyses are shown in Table 4. All analyses yielded essentially the same accuracy and precision for the parameters of interest, although the recovery of r_∞ for the unconstrained analysis with linking schemes A and B is somewhat inferior because of a larger standard deviation. The constrained analyses yielded estimates for $\kappa(90°)$ and, hence, for G_r with more significant digits. Essentially similar results were obtained with the simulation values $\tau^t = 8$ ns, $\Phi^t = 8$ ns, $\beta^t = 0.10$, $r_\infty{}^t = 0.20$, $\tau_r{}^t = 1$ ns, and $G^t = 1.0$ (results not shown). In all cases the results were found to be independent of the initial guesses for the nonlinear least-squares search.

The use of fixing r_0 or G to *a priori* values was investigated in more detail. Polarized decay curves were generated by using the simulation values $\tau^t = 5$ ns, $\Phi^t = 5$ ns, $\beta^t = 0.10$, $r_\infty{}^t = 0.20$, $\tau_r{}^t = 1$ ns, and $G^t = 1.0$ at a time increment of 62 ps. Two sets of analyses were performed. In the first set, linking scheme C_1 was used and $\kappa(90°)$ was fixed at various values ranging from 0.93 to 1.08 while r_0 was freely adjustable, i.e., both β and r_∞ were freely adjustable without constraint. The χ_g^2 value was 0.942 in all cases. The estimates for τ, Φ, and β were in very good agreement with the simulation values, irrespective of the value used for $\kappa(90°)$. The estimate for r_∞ increased with increasing values for $\kappa(90°)$ and ranged from 0.175 to 0.231. The relation between the recovered values for r_0, r_∞, β, and the fixed G value is shown in Figure 1. In the second set of analyses, linking scheme B was used and r_0 was fixed at various values from 0.28 to 0.32. Again, the estimates were in good agreement with the simulation values except for the parameter r_∞. The observed relation between the recovered values for r_∞, β, $\kappa(90°)$, or equivalently G and the fixed value for r_0 is shown in Figure 1.

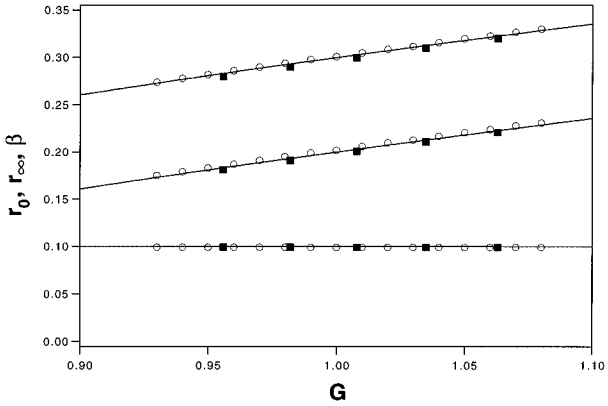

Figure 1. Relation between the values for r_0, r_∞, β, and G ($=\kappa(90°)$) for case 2 ($\tau^t = 5$ ns, $\Phi^t = 5$ ns, $\beta^t = 0.10$, $r_\infty{}^t = 0.20$, $\tau_r{}^t = 1$ ns, and $G^t = 1.0$): results obtained when G is fixed at various values in analysis scheme C_1 (○) or when r_0 is fixed at various values in analysis scheme B (■). The solid lines correspond to theoretical curves obtained by using eq 21.

The observed relation between r_0, r_∞, β, and G can be estimated theoretically as follows. If the incorrect values $\kappa^e(0°)$ and $\kappa^e(90°)$ are used instead of the true values $\kappa^t(0°)$ and $\kappa^t(90°)$, the corresponding anisotropy $r^e(t)$ is given by

$$r^e(t) = \frac{i_{||}{}^e(t)/\kappa^e(0°) - i_{\perp}{}^e(t)/\kappa^e(90°)}{i_{||}{}^e(t)/\kappa^e(0°) + 2i_{\perp}{}^e(t)/\kappa^e(90°)} \tag{17}$$

By using

$$i_{||}{}^e(t) = \kappa^t(0°)\, i_{||}{}^t(t) \tag{18}$$

$$i_{\perp}{}^e(t) = \kappa^t(90°)\, i_{\perp}{}^t(t) \tag{19}$$

one has that

$$r^e(t) = \frac{i_{||}{}^t(t)\, \kappa^t(0°)/\kappa^e(0°) - i_{\perp}{}^t(t)\, \kappa^t(90°)/\kappa^e(90°)}{i_{||}{}^t(t)\, \kappa^t(0°)/\kappa^e(0°) + 2i_{\perp}{}^t(t)\, \kappa^t(90°)/\kappa^e(90°)} \tag{20}$$

Rearranging and defining $\rho = G^t/G^e$ leads to

$$r^e(t) = \frac{1 + 2r^t(t) - \rho[1 - r^t(t)]}{1 + 2r^t(t) + 2\rho[1 - r^t(t)]} \tag{21}$$

Consideration of eq 21 at $t = 0$ and at infinite time yields the relationships that are represented graphically in Figure 1. The calculated relations compare well with the observed data.

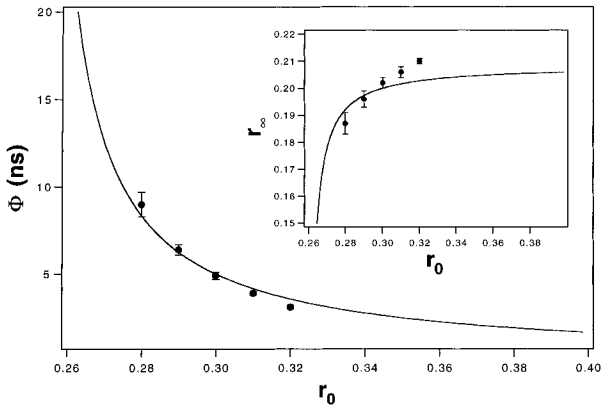

Figure 2. Dependence of Φ and r_∞ on r_0 when r_0 is kept fixed at various values when $G = G^t$. The symbols refer to the results obtained from the simulations (Table 6). The solid lines correspond to eqs A1 and A6.

Equation 21 indicates that in general $r^e(t)$ cannot be expressed as a sum of exponentially decaying functions. However, $r^e(t)$ can be well approximated by a single exponential with essentially the same relaxation time as $r^t(t)$. This can be rationalized as follows. The values for r_0 and r_∞ in $r^e(t)$ depend almost linearly on ρ, and their linear approximations have essentially the same slopes (see Figure 1). This holds for intermediate times as well. Apparently, the effect of ρ is to add/subtract a constant value to/from $r^t(t)$ so that β and Φ are almost independent of ρ and, therefore, practically equal to the true values.

The strong correlation between r_0 and G implies that these parameters contain essentially the same information. When both are fixed in the analysis, the parameter estimates will be correct only if both are fixed to the true value. If one of them is kept fixed to an incorrect value, the freely adjustable parameters will have to adapt to an incorrect value during the nonlinear least-squares search.

The simulated decay curves used in the construction of Figure 1 were reanalyzed by fixing r_0 and G. In the first set of analyses according to scheme C_1, the value of G was fixed to the same set of values as for Figure 1, while r_0 was fixed to the true value. A reduced set of recovered parameter values is shown in Table 5. The value of the fluorescence lifetime is not influenced. With increasing values of G the parameter β decreases, leading to a corresponding increase in r_∞ because r_0 was kept fixed. The value of the parameter Φ and the standard deviation of this estimate increase with increasing values of G. In the second set of analyses according to scheme C_2, the initial anisotropy r_0 was fixed at various values while G was kept fixed at the true value. The results are shown in Table 6. With increasing values of r_0, the estimates for β and r_∞ increase while the value for the parameter Φ decreases. A small change in r_0 (e.g., 6.5%) leads to a large change in Φ (more than 60%). It is shown in the Appendix that the dependence of Φ and r_∞ on r_0 can be estimated from analytical calculations. The calculated and observed dependencies are compared in Figure 2.

The results in Tables 5 and 6 show that, even when the χ_g^2 values are acceptable, incorrect parameter values are obtained when both r_0 and G are fixed and one of them is fixed to an incorrect value. Therefore, it can be stated that when there is some doubt about the value of either r_0 or G it is preferable to use analysis scheme A or B when only r_0 is known precisely or to use analysis scheme C_1 or C_2 when only G is known correctly.

TABLE 5: Influence of Fixing the *G* Factor to a Value Different from G^t in Analysis Scheme C_1[a]

τ (ns)	β	Φ (ns)	r_∞	$G_r = \kappa(90°)$	χ_g^2
4.985	0.112	2.9	0.188	0.94	1.096
(0.005)	(0.001)	(0.1)	(0.001)		
4.988	0.107	3.4	0.193	0.96	1.010
(0.005)	(0.001)	(0.1)	(0.001)		
4.990	0.102	4.1	0.198	0.98	0.956
(0.005)	(0.002)	(0.1)	(0.002)		
4.991	0.098	4.9	0.202	1.00	0.941
(0.005)	(0.002)	(0.2)	(0.002)		
4.992	0.095	5.9	0.205	1.02	0.97
(0.005)	(0.002)	(0.3)	(0.002)		
4.992	0.093	7.4	0.207	1.04	1.049
(0.005)	(0.003)	(0.4)	(0.003)		
4.991	0.094	9.7	0.206	1.06	1.185
(0.005)	(0.005)	(0.8)	(0.005)		
4.989	0.098	13	0.202	1.08	1.385
(0.006)	(0.008)	(2)	(0.008)		

[a] The sum of β and r_∞ is constrained to r_0^t. [b] $\tau^t = 5$ ns, $\Phi^t = 5$ ns, $r_0^t = 0.3$, $\beta^t = 0.1$, $r_\infty^t = 0.20$, $\tau_r^t = 1$ ns, and $G^t = 1$. Time increment is 62 ps. Standard deviations of the parameter estimates are given in parentheses.

TABLE 6: Influence of Constraining the Sum of β and r_∞ to a Value Different from r_0^t in Analysis Scheme C_2 Using G^t [a]

τ (ns)	β	Φ (ns)	r_∞	r_0[b]	$100(r_0 - r_0^t)/r_0^t$	χ_g^2
4.994	0.093	9.0	0.187	0.28	−6.7	1.145
(0.005)	(0.004)	(0.7)	(0.004)			
4.993	0.094	6.4	0.196	0.29	−3.3	0.992
(0.005)	(0.003)	(0.3)	(0.003)			
4.991	0.098	4.9	0.202	0.30	0	0.941
(0.005)	(0.002)	(0.2)	(0.002)			
4.988	0.104	3.9	0.206	0.31	3.3	0.969
(0.005)	(0.002)	(0.1)	(0.002)			
4.984	0.110	3.1	0.210	0.32	6.7	1.058
(0.005)	(0.001)	(0.1)	(0.001)			

[a] $\tau^t = 5$ ns, $\Phi^t = 5$ ns, $r_0^t = 0.3$, $\beta^t = 0.1$, $r_\infty^t = 0.20$, $\tau_r^t = 1$ ns, and $G^t = 1$. Time increment is 62 ps. Standard deviations of the parameter estimates are given in parentheses. [b] The value to which the sum of β and r_∞ is constrained.

The recovery of Φ is related to the ratio Φ/τ. In the next section, the parameter recovery for various Φ/τ ratios is investigated.

CASE 3: $f(t) = \alpha \exp(-t/\tau)$ and $r(t) = (r_0 - r_\infty) \exp(-t/\Phi) + r_\infty$, with Φ^t/τ^t Different from 1. In the previous case the values for the fluorescence lifetime and the rotational correlation time were identical. This is considered to be a favorable situation when there is no r_∞.[24,49] To explore the performance of the various analysis schemes in the presence of nonvanishing r_∞, simulations were performed at the following Φ^t/τ^t ratios: 0.1, 3, and 10. The simulation values $\tau^t = 5$ ns, $\beta^t = 0.10$, $r_\infty^t = 0.20$, $\tau_r^t = 1$ ns, and $G^t = 1$ and a time increment of 62 ps were used in all cases. For each of the linking schemes considered, the generated decay traces were analyzed with freely adjustable and fixed r_0. The results are shown in Tables 7−9.

For all cases the fluorescence lifetime was well recovered. For $\Phi^t/\tau^t = 0.1$ (Table 7), the parameters τ, β, and Φ were equally well recovered by the various analysis schemes. When β and r_∞ were freely adjustable, the accuracy on r_∞ was much better for linking schemes C_1 and C_2. When the sum $\beta + r_\infty$ was constrained, the accuracy on r_∞ for schemes A and B improved substantially but remained inferior to the accuracy obtained with schemes C_1 and C_2.

For $\Phi^t/\tau^t = 3$ (Table 8) and when β and r_∞ were freely adjustable, τ, β, and Φ were well recovered within all schemes. Schemes A and B did not perform well in the recovery of r_∞,

TABLE 7: Recovered Parameters of a Monoexponential $f(t)$ and a Monoexponential $r(t)$ with a Nonvanishing r_∞ and $\Phi^t/\tau^t = 0.1$[a]

scheme	τ (ns)	β	Φ (ns)	r_∞	$G_r = \kappa(90°)$	χ_g^2
	Case A: β and r_∞ Are Freely Adjustable Parameters					
A	4.989	0.100	0.50	0.20	1.0	0.997
	(0.004)	(0.005)	(0.04)	(0.04)	(0.1)	
B	4.988	0.100	0.50	0.21	1.0	0.976
	(0.005)	(0.005)	(0.04)	(0.07)	(0.2)	
C_1	4.987	0.100	0.50	0.1996	1.003	0.975
	(0.005)	(0.005)	(0.04)	(0.0007)		
C_2	4.987	0.100	0.50	0.1985	1	0.975
	(0.005)	(0.005)	(0.04)	(0.0007)		
	Case B: β and r_∞ Are Constrained to $\beta + r_\infty = r_0^t$					
A	4.989	0.100	0.50	0.200	1.00	0.996
	(0.004)	(0.005)	(0.04)	(0.005)	(0.01)	
B	4.987	0.100	0.50	0.200	1.00	0.975
	(0.005)	(0.005)	(0.04)	(0.005)	(0.01)	
C_1	4.987	0.1004	0.50	0.1996	1.003	0.974
	(0.005)	(0.0007)	(0.03)	(0.0007)		
C_2	4.987	0.1014	0.49	0.1986	1	0.974
	(0.005)	(0.0007)	(0.02)	(0.0007)		

[a] $\tau^t = 5$ ns, $\Phi^t = 0.5$ ns, $\beta^t = 0.10$, $r_\infty{}^t = 0.20$, $\tau_r{}^t = 1$ ns, and $G^t = 1$. Time increment per channel = 62 ps.

TABLE 8: Recovered Parameters of a Monoexponential $f(t)$ and a Monoexponential $r(t)$ with a Nonvanishing r_∞ and $\Phi^t/\tau^t = 3$[a]

scheme	τ (ns)	β	Φ (ns)	r_∞	$G_r = \kappa(90°)$	χ^2
	Case A: β and r_∞ Are Freely Adjustable Parameters					
A	4.983	0.10	15	0.29	1.3	0.999
	(0.006)	(0.01)	(3)	(0.04)	(0.1)	
B	4.96	0.09	15	0.4	1.8	1.029
	(0.03)	(0.02)	(3)	(0.2)	(0.9)	
C_1	4.996	0.10	15	0.19	0.992	1.030
	(0.005)	(0.01)	(3)	(0.01)		
C_2	4.995	0.10	15	0.20	1	1.029
	(0.005)	(0.01)	(3)	(0.01)		
	Case B: β and r_∞ Are Constrained to $\beta + r_\infty = r_0^t$					
A	4.992	0.10	16	0.20	1.005	1.002
	(0.004)	(0.01)	(3)	(0.01)	(0.004)	
B	4.995	0.10	15	0.20	1.004	1.029
	(0.005)	(0.01)	(3)	(0.01)	(0.004)	
C_1	4.996	0.092	11	0.208	0.992	1.039
	(0.005)	(0.006)	(1)	(0.006)		
C_2	4.995	0.097	14	0.203	1	1.030
	(0.005)	(0.008)	(2)	(0.006)		

[a] $\tau^t = 5$ ns, $\Phi^t = 15$ ns, $\beta^t = 0.10$, $r_\infty{}^t = 0.20$, $\tau_r{}^t = 1$ ns, and $G^t = 1$. Time increment per channel = 62 ps.

but schemes C_1 and C_2 did. Again, constraint of the sum $\beta + r_\infty$ improved the recovery of r_∞ by schemes A and B substantially.

For $\Phi^t/\tau^t = 10$ (Table 9), none of the analysis schemes was able to recover the anisotropy parameters, although the χ_g^2 values were acceptable. The estimates exhibited large standard deviations. Constraint of the sum $\beta + r_\infty$ did not improve the parameter recovery. It should be emphasized that schemes C_1 and C_2 also did not allow a good recovery.

These results should be compared with those reported in a previous paper where a similar case was considered but with $r_\infty = 0$ (and $r_0 = 0.35$; see Tables 1 and 2 in ref 24). In that case and without constraint, the values of τ, β, and Φ were well recovered with low errors using scheme B for $0.01 < \Phi/\tau < 5$. When r_0 was constrained, the range of allowable Φ/τ values increased: $0.002 < \Phi/\tau < 40$. The results in Tables 7−9 suggest that these ranges are reduced in the case of nonvanishing r_∞. Therefore, it might be expected that the parameter recovery depends on the value of r_∞. For Φ^t/τ^t equal to 0.1, 1, 3, and 10, simulated decay traces were generated by

TABLE 9: Recovered Parameters of a Monoexponential $f(t)$ and a Monoexponential $r(t)$ with $r_\infty{}^t = 0.2$ and $\Phi^t/\tau^t = 10$[a]

scheme	τ (ns)	β	Φ (ns)	r_∞	$G_r = \kappa(90°)$	χ^2
	Case A: β and r_∞ Are Freely Adjustable Parameters					
A	4.996	0.1	61	0.2	0.9	1.029
	(0.006)	(0.1)	(83)	(0.2)	(0.3)	
B	5.00	0.1	61	0.2	1	0.961
	(0.06)	(0.1)	(86)	(0.9)	(2)	
C_1	4.995	0.1	61	0.2	1.001	0.959
	(0.005)	(0.1)	(84)	(0.1)		
C_2	4.995	0.1	61	0.2	1	0.959
	(0.005)	(0.1)	(85)	(0.1)		
	Case B: β and r_∞ Are Constrained to $\beta + r_\infty = r_0^t$					
A	4.995	0.1	61	0.2	0.998	1.028
	(0.004)	(0.1)	(85)	(0.1)	(0.003)	
B	4.996	0.1	61	0.2	1.000	0.970
	(0.005)	(0.1)	(74)	(0.1)	(0.003)	
C_1	4.997	0.1	61	0.2	1.001	1.021
	(0.005)	(0.1)	(50)	(0.1)		
C_2	4.995	0.1	61	0.2	1	0.975
	(0.005)	(0.1)	(55)	(0.1)		

[a] $\tau^t = 5$ ns, $\Phi^t = 50$ ns, $\beta^t = 0.10$, $r_\infty{}^t = 0.20$, $\tau_r{}^t = 1$ ns, and $G^t = 1$. Time increment per channel = 62 ps.

TABLE 10: Recovered Parameters of a Monoexponential $f(t)$ and a Monoexponential $r(t)$ with $r_\infty{}^t = 0.05$ and $\Phi^t/\tau^t = 10$[a]

scheme	τ (ns)	β	Φ (ns)	r_∞	$G_r = \kappa(90°)$	χ^2
	Case A: β and r_∞ Are Freely Adjustable Parameters					
A	5.000	0.20	39	0.06	0.89	1.001
	(0.006)	(0.05)	(13)	(0.06)	(0.09)	
B	4.97	0.20	42	0.2	1	0.960
	(0.05)	(0.06)	(17)	(0.3)	(1)	
C_1	4.994	0.21	41	0.09	0.997	0.960
	(0.005)	(0.06)	(14)	(0.06)		
C_2	4.994	0.21	41	0.09	1	0.960
	(0.005)	(0.06)	(14)	(0.06)		
	Case B: β and r_∞ Are Constrained to $\beta + r_\infty = r_0^t$					
A	4.995	0.20	39	0.10	0.999	1.001
	(0.004)	(0.05)	(13)	(0.05)	(0.003)	
B	4.994	0.21	40	0.09	0.999	0.960
	(0.005)	(0.06)	(14)	(0.06)	(0.003)	
C_1	4.994	0.19	36	0.11	0.997	0.960
	(0.005)	(0.04)	(8)	(0.04)		
C_2	4.994	0.22	43	0.08	1	0.959
	(0.005)	(0.05)	(12)	(0.05)		

[a] $\tau^t = 5$ ns, $\Phi^t = 50$ ns, $\beta^t = 0.25$, $r_\infty{}^t = 0.05$, $\tau_r{}^t = 1$ ns, and $G^t = 1$. Time increment per channel = 62 ps.

using the parameter values $\tau^t = 5$ ns, $\beta^t = 0.25$, $r_\infty{}^t = 0.05$, $\tau_r{}^t = 1$ ns, and $G^t = 1$ at a time increment of 62 ps. The results for $\Phi^t/\tau^t = 10$ are shown in Table 10. The reduced value of r_∞ did not allow for a better parameter recovery for any of the considered Φ^t/τ^t ratios. The conclusions remained the same as for the higher r_∞. The results obtained with analysis scheme B with the sum $\beta + r_\infty$ constrained are similar if not identical to the results acquired with the schemes C_1 and C_2. The effect of constraining the sum $\beta + r_\infty$ in the analysis schemes C_1 and C_2 led to a somewhat smaller standard deviation of the parameter estimates. The performance of scheme A is somewhat better than that of scheme B in the unconstrained case. When constraint is used, schemes A and B perform equally well.

For the case $\Phi^t/\tau^t = 10$ with $\tau^t = 5$ ns, $\beta^t = 0.1$, and $r_\infty{}^t = 0.2$, additional simulations were performed to investigate the conditions under which the parameter recovery can be improved. Decays traces were simulated as before, but at time increments of 50 and 100 ps for various values of the total number of counts. The peak counts in the simulated traces at 54.7° were 10 000, 30 000, and 80 000. The data sets were analyzed with scheme B. The results obtained with the simulations at 100 ps

TABLE 11: Parameter Estimates Obtained by Analysis Scheme B of a Monoexponential $f(t)$ and a Monoexponential $r(t)$ with a Nonvanishing r_∞ and $\Phi^t/\tau^t = 10$; Effect of the Number of Counts[a]

peak counts[b]	N[c]	τ (ns)	β	Φ (ns)	r_∞	$G_r = \kappa(90°)$	χ_g^2
Case A: β and r_∞ Are Freely Adjustable Parameters							
10 000	1.7	4.98	0.03	12	0.5	1.9	1.032
		(0.02)	(0.01)	(5)	(0.3)	(1.5)	
30 000	4.9	4.99	0.06	26	0.4	1.5	1.083
		(0.01)	(0.02)	(9)	(0.2)	(0.8)	
80 000	12.9	4.980	0.06	36	0.5	2.1	0.973
		(0.009)	(0.02)	(11)	(0.1)	(0.9)	
Case B: β and r_∞ Are Constrained to $\beta + r_\infty = r_0^t$							
10 000	1.7	4.990	0.04	19	0.26	1.000	1.038
		(0.004)	(0.01)	(10)	(0.01)		
30 000	4.9	5.001	0.07	29	0.23	0.996	1.084
		(0.003)	(0.02)	(10)	(0.02)	(0.002)	
80 000	12.9	4.998	0.09	49	0.21	1.003	0.980
		(0.002)	(0.03)	(17)	(0.03)	(0.001)	

[a] $\tau^t = 5$ ns, $\Phi^t = 50$ ns, $\beta^t = 0.10$, $r_\infty{}^t = 0.20$, $\tau_r{}^t = 1$ ns, and $G^t = 1$. Time increment per channel is 100 ps. [b] Peak counts of $I(54.7°,t)$ in millions. [c] N is the total number of counts in the analysis in millions.

TABLE 12: Parameter Estimates Obtained by Analysis Scheme C_2 of a Monoexponential $f(t)$ and a Monoexponential $r(t)$ with a Nonvanishing r_∞ and $\Phi^t/\tau^t = 10$; Effect of the Number of Counts[a]

peak counts[b]	N[c]	τ (ns)	β	Φ (ns)	r_∞	χ_g^2
Case A: β and r_∞ Are Freely Adjustable Parameters						
10 000	1.7	4.990	0.04	18	0.26	1.038
		(0.004)	(0.01)	(10)	(0.01)	
30 000	4.9	5.001	0.07	29	0.23	1.084
		(0.003)	(0.02)	(10)	(0.02)	
80 000	12.9	4.998	0.09	50	0.21	0.980
		(0.002)	(0.03)	(18)	(0.03)	
Case B: β and r_∞ Are Constrained to $\beta + r_\infty = r_0^t$						
10 000	1.7	4.990	0.04	19	0.26	1.037
		(0.004)	(0.01)	(8)	(0.01)	
30 000	4.9	5.000	0.09	47	0.21	1.087
		(0.003)	(0.03)	(20)	(0.03)	
80 000	12.9	4.999	0.07	32	0.23	0.985
		(0.002)	(0.01)	(6)	(0.01)	

[a] $\tau^t = 5$ ns, $\Phi^t = 50$ ns, $\beta^t = 0.10$, $r_\infty{}^t = 0.20$, $\tau_r{}^t = 1$ ns, and $G^t = 1$. Time increment per channel is 100 ps. [b] Peak counts of $I(54.7°,t)$ in millions. [c] N is the total number of counts in the analysis in millions.

are shown in Table 11. The results obtained with the simulations obtained at 50 ps were very similar. For both time increments the best results were obtained at a high number of counts when r_0 is constrained to the true value. When r_0 was freely adjustable, the recovery of Φ improved with a higher number of counts at both time increments, while the recovery of β and r_∞ remained poor. The simulated data used in the generation of Table 11 were also analyzed with scheme C_2 (see Table 12). In the case of unconstrained r_0, the estimates for β and r_∞ obtained with scheme C_2 are better than those obtained with scheme B, while the estimates for Φ with both schemes are quite comparable. When r_0 is constrained, schemes B and C_2 perform equally well.

The entries at 10 000 counts in Tables 11 and 12 (time increment, 100 ps) can be compared with the results shown in Table 9 (time increment, 62 ps). The results suggest that measurements performed over a larger time window allow for a smaller standard deviation of the parameter estimates.

For the cases considered the simulated decays were properly matched so that $G^t = 1$. We also investigated whether it would be beneficial to have an equal signal to noise ratio for both polarized intensity decays. This implies that the true value of G is now different from unity. The results were essentially similar to those obtained for $G^t = 1$.

Decay traces at additional polarizer angles θ were simulated in an attempt to improve the parameter recovery for the case $\Phi^t/\tau^t = 10$. In addition to the parallel and perpendicular polarized intensity decays, traces were simulated for θ equal to 10°, 30°, 54.7°, 70°, and 80°. Two different cases were simulated: properly matched curves and polarized intensity curves, which had equal counts at the peak. Results similar to those in the previous case were obtained (results not shown).

TABLE 13: Experimental Fits of DPH in DPPC/SUV at 19 °C

scheme	$\alpha_0°/\alpha_{90}°$	τ_1 (ns)	τ_2 (ns)	β	Φ (ns)	r_∞	$G_r = \kappa(90°)$	χ_g^2
Case A: β and r_∞ Are Freely Adjustable Parameters								
A	3.0	10.61	5.6	0.043	4.6	0.32	2.5	1.12
	(0.4)	(0.06)	(0.3)	(0.003)	(0.6)	(0.07)	(0.1)	
B	3.3[b]	10.61	6.0[b]	0.040[b]	4.5	0.10[b]	1.06[b]	1.11
		(0.04)			(0.6)			
C_1	3.2	10.57	5.6	0.043	4.5	0.316	2.48[c]	1.11
	(0.3)	(0.07)	(0.4)	(0.003)	(0.6)	(0.001)		
Case B: β and r_∞ Are Constrained to $\beta + r_\infty = 0.37$								
A	3.0	10.61	5.6	0.042	4.5	0.328	2.526	1.12
	(0.2)	(0.06)	(0.3)	(0.003)	(0.6)	(0.003)	(0.006)	
B	3.2	10.61	5.6	0.043	4.5	0.328	2.53	1.11
	(0.3)	(0.04)	(0.3)	(0.003)	(0.6)	(0.003)	(0.02)	
C_1	3.3	10.56	5.5	0.046	4.5	0.324	2.48[c]	1.11
	(0.2)	(0.06)	(0.2)	(0.001)	(0.3)	(0.001)		

[a] All collected polarized intensity decays have 10 000 counts at the peak. Time increment per channel is 171 ps. [b] Standard deviations not available because of an ill-conditioned matrix at the point of convergence. [c] Calculated from the measured steady-state anisotropy by using eq 14.

Experimental and Simulated Decays Associated with DPH in DPPC/SUV

Polarized intensity decays of DPH in DPPC/SUV at 19° were collected at 0°, 90°, and 54.7° with an equal number of counts at the peak (10 000 counts). The total number of channels for each trace was 511. The time increment per channel was 171 ps. The excitation wavelength was 320 nm and the fluorescence was monitored at 430 nm. A degassed solution of POPOP in ethanol was used as reference ($\tau_f = 1.2$ ns). The measured stationary anisotropy was 0.33 and is similar to the value reported by others [0.33 at 30 °C (Prendergast et al., 1981),[50] 0.30 at 29 °C (Davenport et al., 1986),[51] 0.31 at 30 °C (Genz et al., 1986),[52] 0.32 at 20 °C(Kimura and Ikegami, 1985)[53]]. The G_f factor was calcuated by using eq 14.

The decays were analyzed according to schemes A, B, and C_1. The results are shown in Table 13. The total fluorescence decay was found to be biexponential in accordance with other reports.[10,14,15,50,51] When β and r_∞ are freely adjustable, the parameter estimates obtained with schemes A and C_1 are very similar and different from those obtained with scheme B. The results corresponding with scheme B are not reliable because of ill-conditioned matrices during the least-squares search. This is reflected by the lack of availability of obtaining all of the standard deviations. The value recovered for G_r by scheme A corresponded well with the value of G_f used in scheme C_1. The rather high value for r_∞ is expected because the experiments were conducted well below the gel to liquid crystalline phase transition. The data were also analyzed by constraining the sum of β and r_∞ to 0.37. This value is approximately the average of the estimates for r_0 obtained from analyses of several

TABLE 14: Simulations Related to the Experimental Data of DPH in DPPC/SUV in Table 8[a]

scheme	$\alpha_0°/\alpha_{90}°$	τ_1 (ns)	τ_2 (ns)	β	Φ (ns)	r_∞	$G_r = \kappa(90°)$	χ_g^2
Case A: β and r_∞ Are Freely Adjustable Parameters								
A	4.2	10.42	4.8	0.051	5.1	0.29	2.5	1.039
	(0.4)	(0.03)	(0.2)	(0.003)	(0.6)	(0.06)	(0.4)	
B	4.3	10.41	4.7	0.051	5.1	0.3	2	1.051
	(3)	(0.04)	(0.5)	(0.005)	(0.6)	(0.5)	(3)	
C_1	4.2	10.41	4.7	0.050	5.1	0.318	2.651	1.050
	(0.2)	(0.04)	(0.3)	(0.002)	(0.6)	(0.002)		
C_2	4.2	10.41	4.7	0.050	5.1	0.319	2.656	1.050
	(0.2)	(0.04)	(0.3)	(0.002)	(0.6)	(0.002)		
Case B: β and r_∞ Are Constrained to $\beta + r_\infty = 0.37$								
A	4.2	10.41	4.8	0.050	5.1	0.320	2.66	1.037
	(0.2)	(0.03)	(0.2)	(0.003)	(0.6)	(0.003)	(0.02)	
B	4.2	10.41	4.7	0.050	5.1	0.320	2.660	1.048
	(0.2)	(0.04)	(0.3)	(0.003)	(0.6)	(0.003)	(0.002)	
C_1	4.2	10.41	4.7	0.051	4.8	0.319	2.651	1.049
	(0.2)	(0.04)	(0.3)	(0.001)	(0.4)	(0.001)		
C_2	4.2	10.41	4.7	0.051	4.9	0.319	2.656	1.047
	(0.2)	(0.04)	(0.3)	(0.001)	(0.4)	(0.001)		

[a] $\tau_1^t = 10.6$ ns, $\tau_2^t = 5.5$ ns, $\Phi^t = 4.5$ ns, $\beta^t = 0.05$, $r_\infty^t = 0.32$, $G^t = 2.656$, and $G_f = 2.651$. Time increment per channel is 171 ps.

TABLE 15: Simulations Related to Experimental Data of DPH in DPPC/SUV at 45 °C[a]

scheme	$\alpha_0°/\alpha_{90}°$	τ_1 (ns)	τ_2 (ns)	β	Φ (ns)	r_∞	$G_r = \kappa(90°)$	χ_g^2
Case A: β and r_∞ Are Freely Adjustable Parameters								
A	6.4	7.96	2.4	0.337	1.00	0.05	1.04	1.045
	(0.6)	(0.02)	(0.3)	(0.008)	(0.04)	(0.01)	(0.04)	
B	6.3	7.96	2.5	0.338[b]	1.02[b]	0.11[b]	1.21[b]	1.048
	(0.6)	(0.02)	(0.2)					
C_1	6.1	7.96	2.5	0.337	0.98	0.0384	0.999	1.047
	(0.6)	(0.02)	(0.3)	(0.008)	(0.04)	(0.0008)		
C_2	6.1	7.96	2.5	0.337	0.98	0.0387	1	1.047
	(0.6)	(0.02)	(0.3)	(0.008)	(0.04)	(0.0008)		
Case B: β and r_∞ Are Constrained to $\beta + r_\infty = 0.37$								
A	6.4	7.96	2.5	0.332	1.00	0.038	1.00	1.045
	(0.6)	(0.02)	(0.3)	(0.006)	(0.04)	(0.006)	(0.02)	
B	6.0	7.96	2.5	0.337	0.98	0.033	0.98	1.047
	(0.6)	(0.02)	(0.3)	(0.008)	(0.04)	(0.008)	(0.02)	
C_1	6.2	7.96	2.5	0.3318	1.00	0.0382	0.999	1.046
	(0.6)	(0.02)	(0.3)	(0.0008)	(0.02)	(0.008)		
C_2	6.4	7.96	2.5	0.3314	1.01	0.0386	1	1.046
	(0.6)	(0.02)	(0.3)	(0.0008)	(0.02)	(0.0008)		

[a] $\tau_1^t = 8$ ns, $\tau_2^t = 3$ ns, $(\alpha_0°/\alpha_{90}°)^t = 6.6$, $\Phi^t = 1$ ns, $\beta^t = 0.33$, $r_\infty^t = 0.04$, $G^t = 1$, $G_f = 0.999$. Time increment per channel is 171 ps. [b] Standard deviations not available because of ill conditioned matrix at the point of convergence.

experiments conducted at temperatures below the phase transition. In the case with the constraint $\beta + r_\infty = 0.37$, the results obtained by schemes A, B, and C_1 are very similar and essentially equal to those obtained with schemes A and C_1 in the unconstrained analyses. Use of the constraint allows one to obtain reliable parameter estimates with scheme B. The similarity of the results obtained by the various analyses indicates that the values of $G_f = 2.48$ and $r_0 = 0.37$ are internally consistent (see the section with the simulated data sets in which both the G factor and r_0 are fixed). Experimental data were also collected at a time increment of 66 ps. The corresponding parameter estimates obtained with the various analyses were comparable with those shown in Table 13.

Because the total fluorescence decay of DPH in DDPC/SUV is biexponential, simulated data were generated by mimicking the experimental data set. Each simulated polarized intensity decay had 10 000 counts at the peak. The results obtained with the unconstrained and constrained analyses are shown in Table 14. In the unconstrained analyses the results obtained with the various schemes are comparable. The best precision is obtained with schemes C_1 and C_2. With scheme A, only the precision of r_∞ is inferior to the precisions obtained with schemes C_1 and C_2. The uncertainty in the estimate for r_∞ obtained with scheme B is unacceptably high. In the constrained analyses, all schemes perform equally well. In both the unconstrained and constrained analyses, the estimates for τ_2 and the ratio α_1/α_2 deviate somewhat from their true values. The same deviations were obtained when the decay trace at 54.7° was analyzed separately. Additional polarized decay traces were simulated with $G^t = 1$. These three decay traces were analyzed simultaneously according to scheme C_2, and essentially the same parameter estimates as those shown in Table 14 were obtained.

The experimental data were also analyzed in terms of a nonassociative model with two fluorescence relaxation times and $r(t) = \beta_1 \exp(-t/\Phi_1) + \beta_2 \exp(-t/\Phi_2) + r_\infty$. The estimates for the anisotropy parameters obtained with schemes A, B, and C_1 with and without the constraint on r_0 were of the following magnitudes: $\beta_1 = 0.04$, $\Phi_1 = 7$ ns, $\beta_2 = 0.02$, $\Phi_2 = 0.8$ ns, and $r_\infty = 0.31$. Even in the constrained analysis with C_1 the standard deviations of β_2 and Φ_2 were high: about 50% for β_2 and 100% for Φ_2. Therefore, this model does not seem to be appropriate. This is in agreement with the results reported by Wang et al.,[10] Davenport et al.,[51] and Lakowicz et al.,[54] although other authors found that a multiexponential expression in addition to r_∞ was required for an adequate description of the data.[14,15]

The number of components in an experimentally collected anisotropy decay can be influenced by the time-resolved method used, the analysis programs for the data, and the experimental method used for preparing the samples. With respect to the last condition, it has to be noted that various stationary anisotropy values have been reported for assumed equivalent vesicle systems with the same fluorescent reporter molecules. The stationary anisotropy values that we obtained are in agreement with those reported by several authors (*vide supra*). If experimental procedures can influence the value for stationary anisotropy, the time-resolved anisotropy and the corresponding associated model will be even more sensitive to the experimental conditions.

The performance of the various schemes in the case of an anisotropy decay with a low r_∞ value was investigated by simulations. The simulated parameters were similar to those reported by Ameloot et al.[14] for DPH in DPPC/SUV at 45 °C. The results are shown in Table 15. Without any constraint in the analysis, all parameters were recovered well by schemes A, C_1, and C_2. The accuracy of r_∞ obtained by scheme A is not so good. Scheme B gave good estimates for all of the parameters except for r_∞ and G, and at the point of convergence not all of the standard deviations could be calculated because the corresponding matrix was ill conditioned. When r_0 was constrained to 0.37, all schemes performed well, but the standard deviations of β and r_∞ obtained by schemes C_1 and C_2 were smaller.

Conclusions

It has been shown previously[24] that when $f(t)$ is monoexponential and $r(t)$ does not contain an r_∞ term, the parameters β and Φ are well recovered by global analysis of unmatched polarized intensity decay curves when $0.01 \leq \Phi/\tau \leq 5$ ($\tau = 5$ ns), even when r_0 is not constrained to the true value. In this paper, the parameter recovery from unmatched polarized intensity decay curves in the presence of an r_∞ term was investigated. Two different sets of unmatched traces were considered. The first set consisted of the decay curves at 0°,

54.7°, and 90° (Scheme A), while the second set contained the traces at 0° and 90° (scheme B). For $r_\infty = 0.2$ with $\beta = 0.1$, and for $r_\infty = 0.05$ with $\beta = 0.25$, the following cases were considered: $\Phi/\tau = 0.1$, 1, 3, and 10 ($\tau = 5$ ns). The value obtained for the fluorescence lifetime τ is accurate and precise for all cases considered. For $\Phi/\tau = 0.1$, 1, and 3, the parameters β and Φ are well recovered by both schemes. The accuracy and precision are very similar to the results obtained with matched decay traces. For both values of r_∞, the recovery of r_∞ is not as good compared to the results obtained from matched curves. Scheme A performs somewhat better than scheme B. When the fundamental anisotropy r_0 is fixed to the true value, the analyses with schemes A and B yield the same accuracy and precision as the analysis of the matched curves.

When $\Phi/\tau = 10$, the parameter estimates for the anisotropy parameters are inaccurate and imprecise and suffer from very high uncertainty. No improvement is obtained when r_0 and the matching factor G are kept fixed to the true values. This is in contrast with the results obtained for $r(t)$ without an r_∞ term, where good parameter recovery is obtained at even higher Φ/τ ratios $0.002 \leq \Phi/\tau \leq 40$ ($\tau = 5$ ns) when r_0 or G is kept fixed. There is some improvement when the signal to noise ratio is increased.

In the case of a biexponential $f(t)$ analysis, scheme B requires the additional information about r_0 to yield reliable parameter estimates. Scheme A performs well, but the parameter estimates are less precise than the results obtained by schemes C_1 and C_2.

The global analysis of unmatched polarized intensity decays allows one to compare the information obtained by using a fixed value for r_0 to the information implicitly included in matched decay traces. It can be concluded that, with respect to the normalization of the polarized decay traces, r_0 and G contain the same information. In general, the best accuracy and precision in the parameter recovery are obtained when a predetermined value for G or r_0 is used in the analysis. When G is fixed to an incorrect value while r_0 is freely adjustable (or vice versa), β and Φ were well recovered and the estimate for r_∞ was found to be strongly correlated with the value for G (or r_0). The performance of the analyses without the information about r_0 or G depends more on the Φ/τ ratio than for the analyses where this information is used. Fixation of G and r_0 to the proper value might lead to an improved precision. The use of incorrect values for G (with r_0 freely adjustable) or r_0 (with G freely adjustable) may lead to good data fits, i.e., acceptable χ_g^2 values, although the parameter estimates are incorrect. A small change in r_0 can lead to a large change in Φ. The strong correlation between r_0 and G implies that when both are fixed in the analysis the parameter estimates will be correct only if both are fixed to the true values. If one is kept fixed to an incorrect value, the freely adjustable parameters will have to adapt in the nonlinear least-squares search. It is possible to obtain an acceptable value for χ_g^2 at the point of convergence, although the parameter estimates are not correct. Therefore, it is advisable to fix either G or r_0, but not both, and to compare the parameter estimates for both analyses. Alternatively, the comparison of the results obtained with a freely adjustable G and a fixed G can provide a check for the data analysis.

Acknowledgment. The continuing support of the FKFO and the Ministry of "Wetenschapsbeleid" through Grants IUAP-II-16 and IUAP-III-040 is gratefully acknowledged. We thank N. Boens for the implementation of the global analysis kernel.

Appendix: Derivation of the Dependence of Φ and r_∞ on r_0 When $G = G^t$

The results shown in Table 6 indicate that the fluorescence lifetime τ exhibits a very small but systematic dependence on the value given to r_0 when $G = G^t$. Under the approximation that τ is independent of r_0, the values for Φ and r_∞ in the approximative anisotropy decay, $r^a(t)$, can be estimated as follows.

In the least-squares search, the fitting parameters are determined such that the area under the fitting functions matches the area under the experimental polarized intensity decays.[55] Therefore, under the indicated assumption concerning τ, one can state that the areas under $r^t(t)$ and $r^a(t)$ will be equal within the time window of observation, T. Additional relations for Φ and r_∞ can be obtained by considering the moments g_n:

$$g_n \equiv \int_0^T t^n r(t)\, dt \tag{A1}$$

Evidently, g_0 corresponds to the area under the curve.

By requiring that moments of $r^a(t)$ equal the corresponding moments of $r^t(t)$, we obtain additional relations for Φ and r_∞. Under the condition that $T \geq 5\Phi$, one obtains the following approximations:

$$g_0^{\,t} \approx (r_0 - r_\infty)\Phi + r_\infty T \tag{A2}$$

$$g_1^{\,t} \approx (r_0 - r_\infty)\Phi^2 + r_\infty T^2/2 \tag{A3}$$

$$g_2^{\,t} \approx (r_0 - r_\infty)\Phi^3 + r_\infty T^3/3 \tag{A4}$$

Elimination of Φ from eqs A2 and A3 leads to a quadratic equation in r_∞. Alternatively, use of eqs A2, A3, and A4 leads to

$$r_\infty = \frac{6g_0^{\,t}g_1^{\,t} - 3g_2^{\,t}r_0 - 4(g_0^{\,t})^2T + 4g_1^{\,t}r_0T}{-3g_2^{\,t} + 10g_1^{\,t}T - 5g_0^{\,t}T^2 + r_0T^3} \tag{A5}$$

$$\Phi = \frac{3g_2^{\,t} - 4g_1^{\,t}T + g_0^{\,t}T^2}{6g_1^{\,t} - 4g_0^{\,t}T + r_0T^2} \tag{A6}$$

For the cases considered in Table 6, the relationships expressed by eqs A5 and A6 are similar to those obtained from the acceptable solution of the above-mentioned quadratic equation. The former relationships are shown in Figure 2.

References and Notes

(1) Cundall, R. B., Dale, R. E., Eds. *Time-resolved Fluorescence Spectroscopy in Biochemistry and Biology*; NATO ASI Series A: Life Sciences; Plenum Press: New York, 1983; Vol. 69.

(2) Brand, L.; Knutson, J. R.; Davenport, L.; Beechem, J. M.; Dale, R. E.; Walbridge, D. G.; Kowalczyk, A. A. In *Spectroscopy and the Dynamics of Molecular Biological Systems*; Bayley, P. M., Dale, R. E., Eds.; Academic Press: London, 1985; pp 259−305.

(3) Fleming, G. *Chemical Applications of Ultrafast Spectroscopy*; Oxford University Press: London, 1986.

(4) (a) Dutt, G. B.; Doraiswamy, S.; Periasamy, N. *J. Chem. Phys.* **1991**, *94*, 5360. (b) Dutt, G. B.; Doraiswamy, S.; Periasamy, N.; Venkataraman, B. *J. Chem. Phys.* **1990**, *93*, 8498. (c) Dutt, G. B.; Doraiswamy, S. *J. Chem. Phys.* **1992**, *96*, 2475.

(5) Ben-Amotz, D.; Drake, J. M. *J. Chem. Phys.* **1988**, *89*, 1019.

(6) Quitevis, E. L.; Marcus, A. H.; Fayer, M. D. *J. Phys. Chem.* **1993**, *97*, 5762.

(7) Wittouck, N.; Negri, R. M.; Ameloot, M.; De Schryver, F. C. *J. Phys. Chem.* **1994**, *116*, 10601.

(8) Winnik, M. A., Ed. *Photophysical and Photochemical Tools in Polymer Science. Conformation, Dynamics, Morphology;* NATO ASI Series C: Mathematical and Physical Sciences; Reidel: Dordrecht, 1986; Vol. 182.

(9) Zannoni, C.; Arcioni, A.; Cavatorta, P. *Chem. Phys. Lipids* **1983**, 32, 179.
(10) Wang, S.; Beechem, J. M.; Gratton, E.; Glaser, M. *Biochemistry* **1991**, *30*, 5565.
(11) Samori, B., Thulstrup, E. W., Eds. *Polarized Spectroscopy of Ordered Systems*; NATO ASI Series C: Mathematical and Physical Sciences; Kluwer, Dordrecht: 1988; Vol. 242.
(12) Pap, E. H. W.; ter Horst, J. J.; van Hoek, A.; Visser, A. J. W. G. *Biophys. Chem.* **1994**, *48*, 337.
(13) Van der Sijs, D. A.; Van Faasen, E. E.; Levine, Y. K. *Phys. Chem. Lett.* **1994**, *216*, 559.
(14) Ameloot, M.; Hendricx, H.; Herreman, W.; Pottel, H.; van Cauwelaert, F.; van der Meer, W. *Biophys. J.* **1984,** *46*, 525.
(15) Dale, R. E.; Chen, L. A.; Brand, L. *J. Biol. Chem.* **1977**, *252*, 7500.
(16) Kinosita, K., Jr.; Kawato, S.; Ikewami, A. *Biophys. J.* **1977**, *20*, 289.
(17) Lakowicz, J. R.; Prendergast, F. G. *Science* **1978**, *200*, 1399.
(18) Heyn, M. *FEBS Lett.* **1979**, *108*, 358.
(19) Lipari, G.; Szabo, A. *Biophys. J.* **1980**, *30*, 489.
(20) Szabo, A. *J. Chem. Phys.* **1984**, *81*, 150.
(21) van der Meer, W.; Pottel, H.; Herreman, W.; Ameloot, M.; Hendrickx, H.; Schröder, H. *Biophys. J.* **1984,** *46*, 515.
(22) Beechem, J. M.; Brand, L. *Photochem. Photobiol.* **1986**, *44*, 323.
(23) Beechem, J. M.; Gratton, E.; Ameloot, M.; Knutson, J. R.; Brand, L. In *Topics in Fluorescence Spectroscopy*; Lakowicz, J. R., Ed.; Plenum Press: New York, 1991; Vol. 2, pp 241−305.
(24) Crutzen, M.; Ameloot, M.; Boens, N.; Negri, R. M.; De Schryver F. C. *J. Phys. Chem.* **1993**, *97*, 8133.
(25) Demas, J. N. *Excited State Lifetime Measurements*; Academic Press: New York, 1983.
(26) O'Connor, D. V.; Phillips, D. *Time-correlated Single Photon Counting*; Academic Press: London, 1984.
(27) Lakowicz, J. R., Ed. *Topics in Fluorescence Spectroscopy*; Plenum Press: New York, 1991; Vol. 1.
(28) Wahl, Ph. *Biophys. Chem.* **1979**, *10*, 91.
(29) Ricka, J. *Rev. Sci. Instrum.* **1981,** *52*, 195.
(30) Dale, R. E. In *Time-Resolved Fluorescence Spectroscopy in Biochemistry and Biology*; Cundall, R. B., Dale, R. E., Eds.; NATO ASI Series A: Life Sciences; Plenum Press: New York, 1983; Vol. 69, pp 555−612.
(31) Gilbert, C. W. In *Time-Resolved Fluorescence Spectroscopy in Biochemistry and Biology*; Cundall, R. B., Dale, R. E., Eds.; NATO ASI Series A: Life Sciences; Plenum Press: New York, 1983; Vol. 69, pp 605−606.
(32) Ameloot, M.; Hendrickx, H. *Biophys. J.* **1983**, *44*, 27.
(33) Arcioni, A.; Zannoni, C. *Chem. Phys.* **1984**, *88*, 113.
(34) Cross, A.; Fleming, G. R. *Biophys. J.* **1984**, *46*, 45.
(35) Beechem, J. M.; Ameloot, M.; Brand, L. *Anal. Instrum.* **1985**, *14*, 379.
(36) Flom, S. R.; Fendler, J. H. *J. Phys. Chem.* **1988**, *92*, 5908.
(37) Marsh, A. J.; Rumbles, G.; Soutar, I.; Swanson, L. *Chem. Phys. Lett.* **1992**, *195*, 31.
(38) André, J. C.; Bouchy, M.; Viovy, J. L.; Vincent, L. M.; Valeur, B. *Computers Chem.* **1982**, *6*, 5.
(39) Waxman, E.; Laws, W. R.; Laue, T. M.; Nemerson, Y.; Ross, J. B. A. *Biochemistry* **1993**, *32*, 3005.
(40) Khalil, M. M.; Boens, N.; Van der Auweraer, M.; Ameloot, M.; Andriessen, R.; Hofkens, J.; De Schryver, F. C.; *J. Phys. Chem.* **1991**, *95*, 9375.
(41) Gauduchon, P.; Wahl, Ph. *Biophys. Chem.* **1978**, *8*, 87.
(42) Wijnaendts van Resandt, R. W.; Vogel, R. H.; Provencher, S. W. *Rev. Sci. Instrum.* **1982**, *53*, 1392.
(43) Zuker, M.; Szabo, A. G.; Bramall, L.; Krajcarski, D. T.; Selinger, B. *Rev. Sci. Instrum.* **1985**, *56*, 14.
(44) Kolber, Z. S.; Barkley, M. D. *Anal. Biochem.* **1986**, *152*, 6.
(45) Boens, N.; Ameloot, M.; Yamazaki, I.; De Schryver, F. C. *Chem. Phys.* **1988**, *121*, 73.
(46) Boens, N.; Janssens, L. D.; De Schryver, F. C. *Biophys. Chem.* **1989**, *33*, 77.
(47) Marquardt, D. W. *J. Soc. Ind. Appl. Math.* **1963**, *11*, 431.
(48) Van den Zegel, M.; Boens, N.; Daems, D.; De Schryver, F. C. *Chem. Phys.* **1986**, *101*, 311.
(49) Wahl, Ph. *Chem. Phys.* **1977**, *22*, 245.
(50) Prendergast, F. G.; Haugland, R. P.; Callahan, P. J. *Biochemistry* **1981**, *20*, 7333.
(51) Davenport, L.; Kuntson, J. R.; Brand, L. *Biochemistry* **1986**, *25*, 1811.
(52) Genz, A.; Holzwarth, J. F.; Tsong, T. Y. *Biophys. J.* **1986,** *50*, 1043.
(53) Kimura, Y.; Ikegami, A. *J. Membr. Biol.* **1985**, *85*, 225.
(54) Lakowicz, J. R.; Cherek, H.; Maliwal, B. P.; Gratton, E. *Biochemistry* **1985**, *24*, 376.
(55) Awaya, T. *Nucl. Instrum. Methods* **1979**, *165*, 317.

JP960085J